Electronic Supplementary Material (ESI) for ChemComm.

Supporting Information

Electrochemically-derived graphene oxide membrane with high stability and superior ionic sieving

Pei Yu[a], Zhiyuan Xiong[a, b], Hualin Zhan[b], Ke Xie[b], Yu Lin Zhong[c], George P. Simon[a], and Dan Li[a, b]*

a. Department of Materials Science and Engineering, Monash University, Clayton, Victoria, Australia.

b. Department of Chemical Engineering, University of Melbourne, Parkville, Victoria, Australia.

c. Centre for Clean Environment and Energy, School of Environment and Science, Gold Coast Campus, Griffith University, Gold Coast, Queensland 4222, Australia

ESI-1. Experimental section

Materials. Graphite foil was purchased from Sigma-Aldrich (Product No. GF82433538, thickness 0.2 mm) and used as the graphite source for the synthesis of electrochemically-derived graphene oxide (EGO). Reagent grade sulfuric acid H_2SO_4 (95% - 98%) was purchased from Sigma-Aldrich (Product No. 435589). Analytical reagent sodium chloride was purchased from Chem-Supply (Product No. SA046, 99.7%). Magnesium chloride hexahydrate was received from Merck. Rhodamin B and methylene blue were purchased from Sigma-Aldrich. Ultrapure water (from Millipore Direct-Q system) was used in all relevant experiments.

Sample preparation. EGO was synthesized by the electrochemical oxidation of graphite foil in a two-electrode Tee-cell.[1] Graphite foil with a thickness of 0.2 mm was cut into a round disc (diameter 13 mm, weight 30 mg). The graphite foil was pressed onto a round platinum plate, which served as the working electrode, whilst another round platinum plate was used as the counter electrode. Five pieces of glass fiber membrane filters (Toyo Roshi Kaisha, Ltd. GA-55) were employed as the separator, sandwiched between the working and counter electrodes which were connected to a potentiostat (VMP300, Bio-Logic). In the electrochemical oxidation process, a constant current (2 mA) was applied to the working electrode for 22 hours, with 12 M sulfuric acid solution was employed as the electrolyte. The voltage change during the whole electrochemical process was recorded with time. After the electrochemical oxidation of graphite foil for 22 hours, the samples were taken out and dispersed in water using agitation for a few minutes. The dispersion was washed by the centrifugation process repeatedly until the pH of the dispersion was around 7. After washing, EGO dispersion was subject to ultrasonication for 30 minutes via an ultrasonic probe (Branson Digital Sonifier S450D, 1/2" Horn, 500W, 30% amplitude). The ultrasonicated EGO dispersion was subsequently centrifuged at 4400 rpm. for 1 hour to remove large or non-exfoliated sheets. The weight percentage for remaining EGO after centrifugation was around 75%. CGO was produced by a modified Hummers method originally reported by Kovtyukhaova et al.[2] The purified CGO dispersion was subjected to the same ultrasonication and centrifugation procedure before further use.

Fabrication of EGO membrane. The EGO dispersion (0.5 mg/ml) was filtrated through a polycarbonate membrane (Isopore, 0.1 µm pore size, Sigma-Aldrich) by vacuum filtration. When the filtration was complete, the membrane was dried under vacuum conditions at room temperature for about 24 hours. Following this, the membrane was able to be peeled off the polycarbonate filter for further characterization. CGO membrane were fabricated using the same procedures.

Stability tests. To test the stability, EGO and CGO membranes were fabricated with the same mass loading of 0.6 mg/cm^2 and cut into round pieces with a diameter of 13 mm. Acidic (pH=1.5) or basic (pH=10.5) aqueous solutions were prepared by modifying ultrapure water (pH=6.8) with appropriate amounts of HCl or NaOH. During the stability test, both EGO and CGO membranes were immersed in acidic, neutral and basic aqueous solution for 1 week. After immersion for a certain time (e.g. 24 hours), the membranes in the solution were stirred by a vortex mixer (VELP Scientifica) at a speed of 400 rpm for 1 minute.

Characterization. The structures of EGO and CGO membranes in the dried and wet states, for different immersion times, were characterized by X-ray diffraction (XRD) measurements. EGO and CGO membranes for measurements have the same weight and same mass loading. XRD was performed in a Bruker D2 Phaser diffractometer with a Cu Kα radiation (k = 1.5418 Å). Raman spectroscopy was measured on a Renishaw InVia Raman Microscope with a laser wavelength of 532 nm and a laser spot size of 10 µm. X-ray photoelectron spectroscopy (XPS) was conducted on a VG ESCALAB220i-XL spectrometer which is equipped with a hemispherical analyser. For incident radiation, monochromatic Al Kα X-rays (1486.6 eV) was employed at 220 W (22 mA and 10kV). The surface charging effect was compensated by a low energy flood gun. Thermogravimetric analysis (TGA) of EGO or CGO was conducted by using a Thermo thermogravimetry/differential thermal analyser (TG/DTA) 6300 in the atmosphere of air using a heating rate of 1 °C/min. Zeta potential of the dispersion was performed by Malvern Zetasizer Nano ZS analyser. Atomic force microscopy (AFM) images of EGO sheets were taken by a Bruker Dimension Icon AFM in a tapping mode. For sample preparation, EGO dispersion with 0.01 mg/ml was drop-casted on a Si wafer and dried at 50 °C. Scanning electron microscopy (SEM) images was taken by the JEOL 7001F Field Emission Scanning Election Microscope with an accelerating voltage of 15 kV. Energy dispersive Spectroscopy (EDS) of EGO and CGO was measured by the Oxford instruments X-Max 80 EDS detector equipped on the SEM.

Permeation and nanofiltration test. EGO or CGO membranes were fabricated by a Sterlitech dead-end filtration cell with a compressed air and dried in air for overnight. For concentration-driven permeation tests, a device with a feed reservoir and a permeate reservoir on each side of a membrane clamp was used. EGO and CGO membranes (0.3 mg/cm^2) with a polycarbonate filter as a substrate were fabricated from 0.05 mg/ml EGO or CGO dispersions. The membrane was then assembled in the device using a membrane clamp with an exposure diameter of 4.9 mm. The feed reservoir was filled with 50 ml of feed solution (0.1 M NaCl, 0.1 M $MgCl_2$, 0.02 M methylene blue and 0.02 M Rhodamine B). The permeate reservoir was filled with 50 ml ultrapure water. Solution conductance change was monitored in the permeate reservoir to measure the diffusion of NaCl and $MgCl_2$. UV-Vis spectroscopy was used to monitor the concentration of methylene blue and Rhodamine B.

For the nanofiltration testing, the Sterlitech dead-end filtration cell was used to monitor water filtration through EGO or CGO membrane with different mass loadings. For the rejection test, 1.0 M NaCl, 1.0 M $MgCl_2$, 0.04 mM MB and 0.04 mM RB were filtrated through the EGO or CGO membrane (0.02 mg/cm^2). The conductivities of NaCl and $MgCl_2$ permeates were measured to obtain their rejections. Permeance was monitored by the weight increase of the permeate with time.

ESI-2. Electrochemical process and characterization of EGO

A constant positive current was applied to the graphite electrode and voltage was recorded with oxidation time, as shown in **Figure S1a**. 12 M H_2SO_4 was used as the electrolyte since the product contained the highest yield of EGO compared to other concentrations. From the XRD patterns in **Figure S1b**, the product from 12 M H_2SO_4 shows the lowest graphite peak at around 26.7° and highest peak ratio of EGO to graphite (**Figure S1c**). After centrifugation, the remaining EGO demonstrated no peak in the region around 26° (**Figure S1d**), indicating the complete removal of unoxidized graphite. A stable EGO aqueous dispersion of 4 mg/ml can be obtained from this highly oxidized EGO. After standing for 1 week, the concentration of upper dispersion showed almost no change (**Figure S2a**). AFM images **(Figure S3, S4**) reveal that most EGO sheets are monolayer graphene oxide with a thickness of around 1.2 nm, similar to thickness of CGO sheets (~1.3 nm). The lateral sizes of EGO monolayer sheets were similar to CGO sheets with more than 90% of sheets distributed in the range of 100 – 500 nm (**Figure S4, S5**). From the zeta potential analysis shown in **Figure S2b**, the stable EGO dispersion is maintained due to strong electrostatic stabilization. Although the absolute zeta potential of EGO is lower than that of CGO sheets at the same pH, it is below -30 mV in the pH range of 2.2 – 11.6, which represents sufficiently strong repulsions between the EGO sheets to maintain colloidal stability.[3]

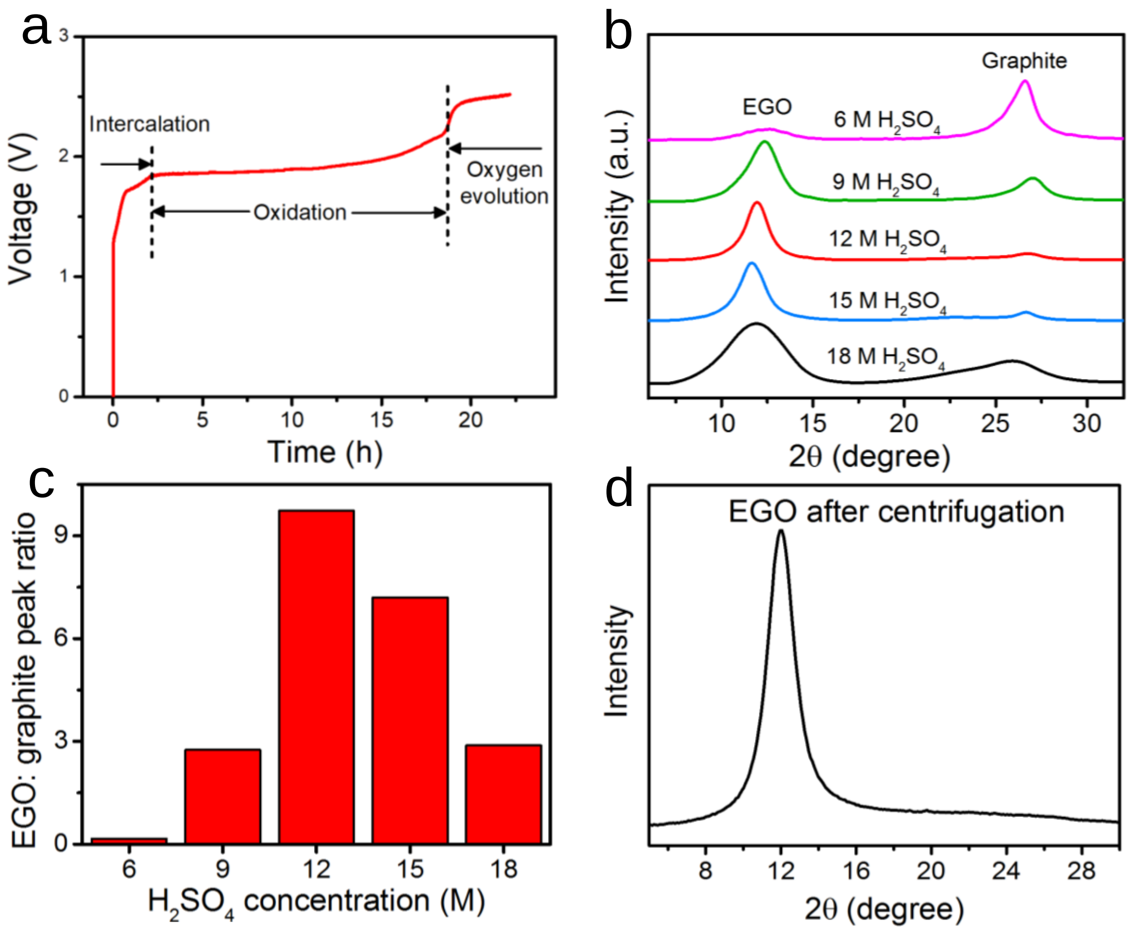

Figure S1. (a) Change in voltage with time during electrochemical oxidation of graphite foil at constant current 2 mA. (b) X-ray diffraction (XRD) patterns of the product from H_2SO_4 of different concentrations. (c) XRD peak ratio of EGO to graphite at different H_2SO_4 concentrations. (d) XRD patterns of the remaining EGO, following after centrifugation.

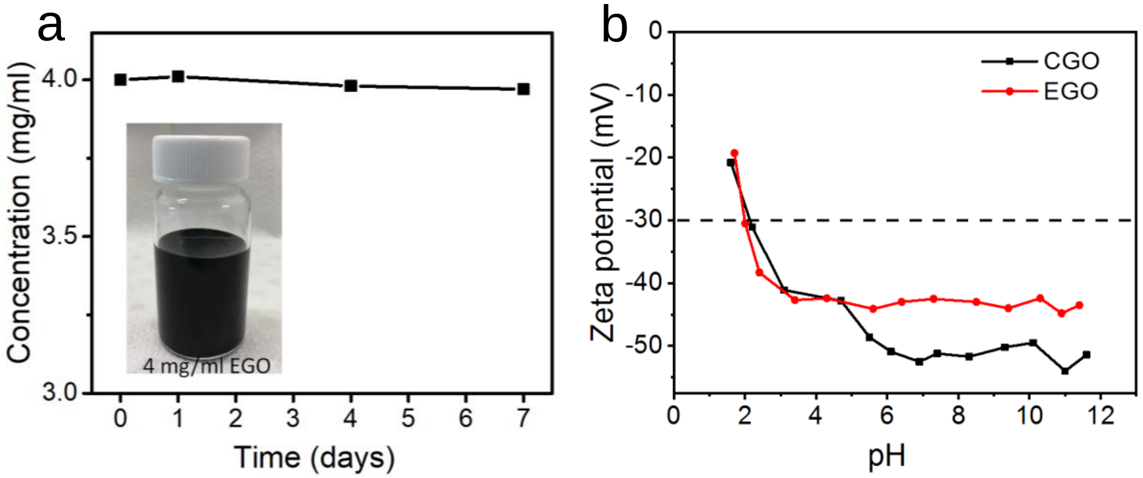

Figure S2. (a) Concentration change of 4 mg/ml EGO dispersion after standing for 1 day, 4 days, 7 days. Image of a 4 mg/ml EGO dispersion. (b) Zeta potentials of EGO and CGO dispersion.

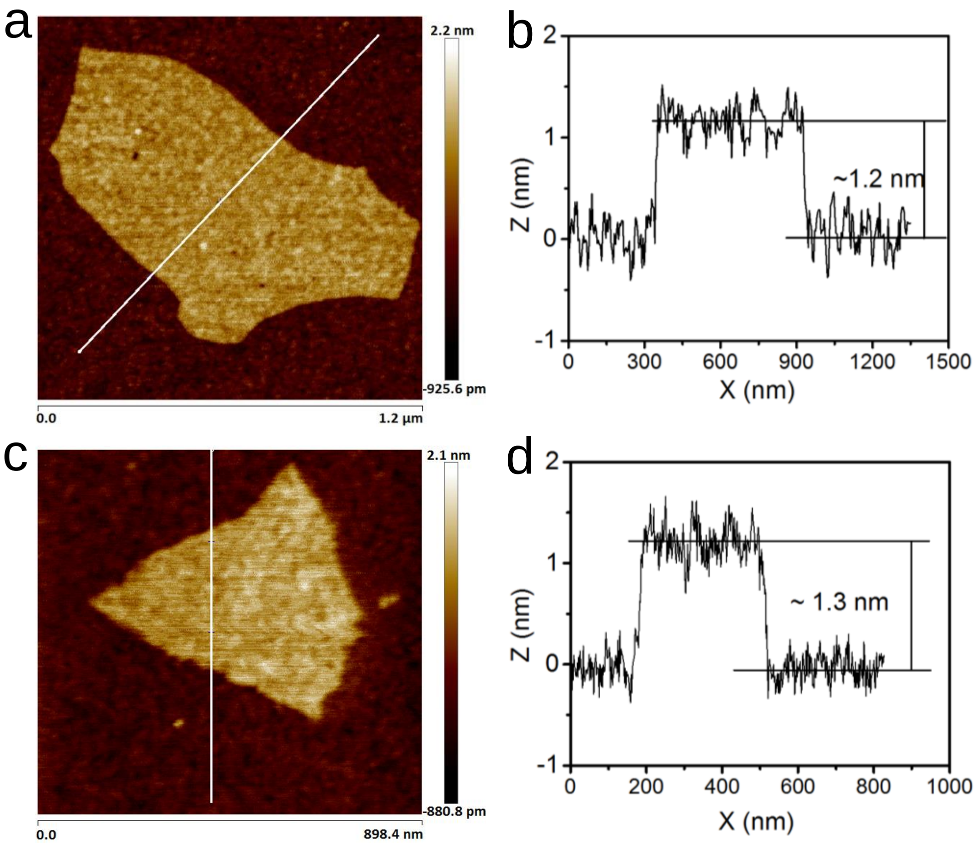

Figure S3. AFM images of (a, b) a typical EGO monolayer and its thickness measurement, (c, d) a typical CGO monolayer and its thickness determination.

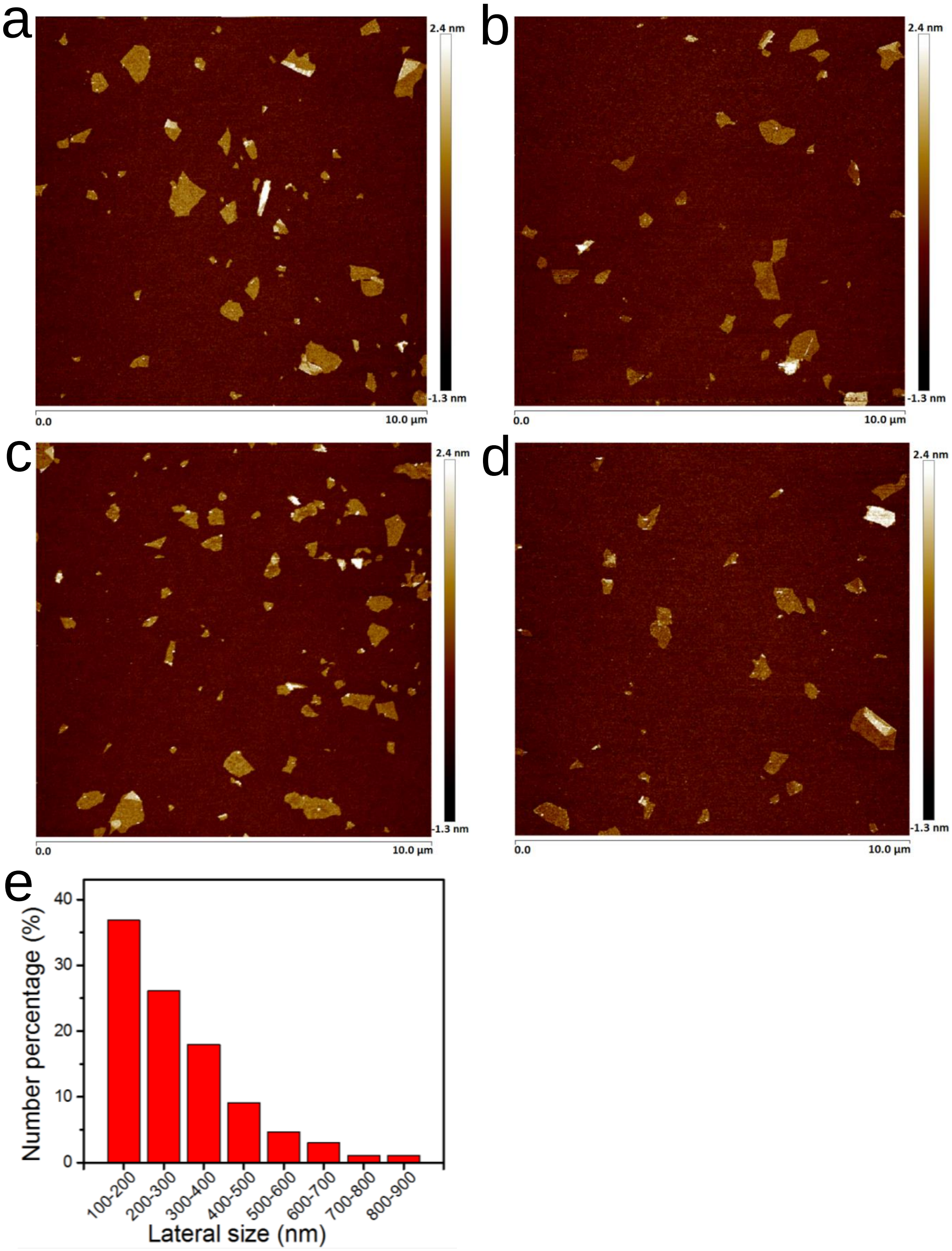

Figure S4. Atomic force microscope (AFM) (a – d) AFM images of EGO sheets deposited on Si wafer. (e) Lateral size distribution of monolayer EGO sheets.

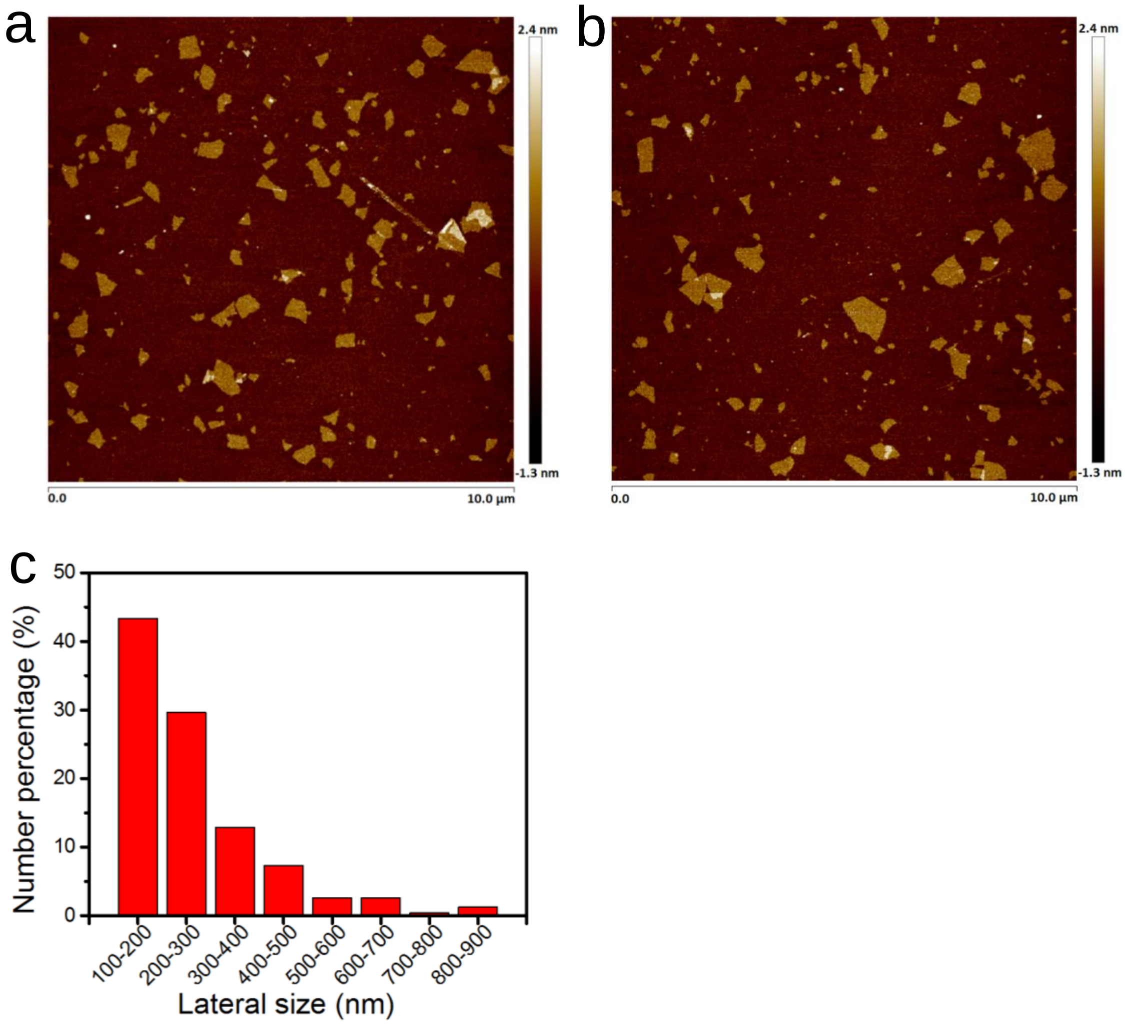

Figure S5. (a, b) AFM images of CGO sheets deposited on a Si wafer. (c) Lateral size distribution of monolayer CGO sheets.

The cross-sections of EGO and CGO membranes were examined by SEM (**Figure S6**). It can be found that EGO and CGO membranes with the same mass loading show very close thicknesses (~2.61 μm and ~2.63 μm, respectively). In addition, both EGO and CGO membranes show a well-aligned multilayered structure. Given the same mass loading and thickness, EGO and CGO should have similar interlayer pore volume.

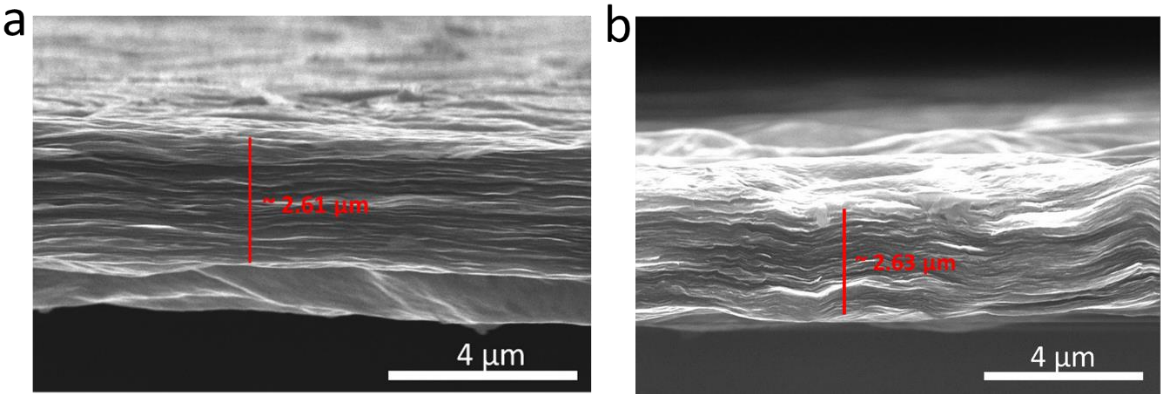

Figure S6. SEM images of (a) EGO membrane cross-section and (b) CGO membrane cross-section with the same mass loading of 0.6 mg/cm^2.

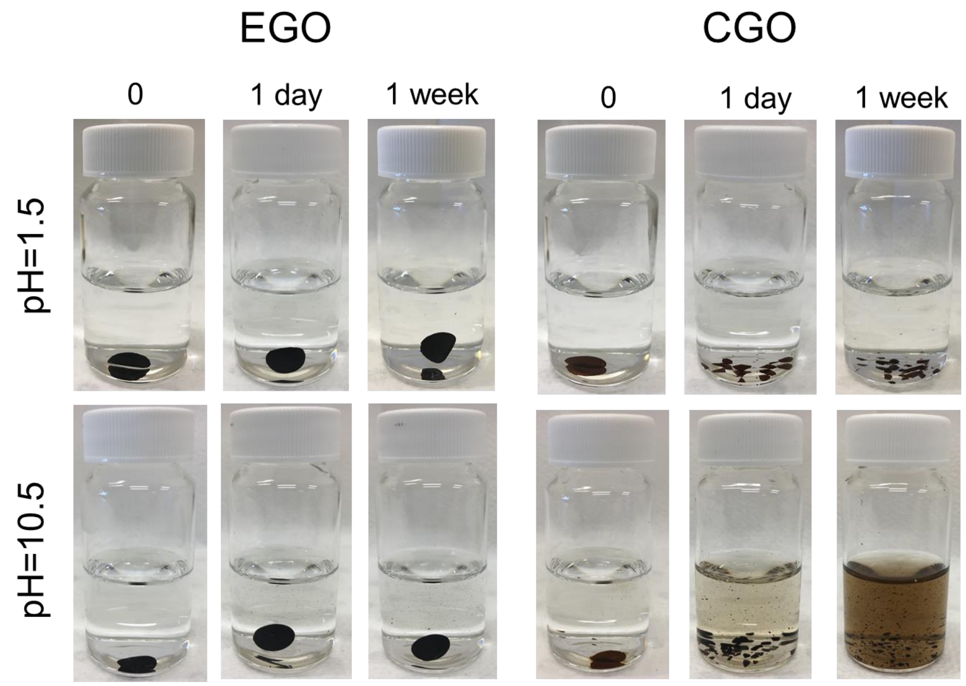

Figure S7. Stability of EGO and CGO membrane in acid and base aqueous dispersions with pH=1.5 and pH=10.5.

ESI-3. XRD analysis for structural change of EGO and CGO membranes with immersion time

Swelling of GO membranes results from the insertion of water molecules between GO sheets, leading to an increasing number of water layers.[4-6] Previous research has correlated the number of intercalated water molecules between GO layers with the interlayer distance obtained by XRD and found that a hydrated GO membrane with an interlayer distance of about 13 Å contained three layers of water molecules between the two GO sheets.[6] From the XRD patterns of EGO membrane immersed in water for 1 minute, a non-symmetrical peak can be observed which contains the transition states between fully dried and fully hydrated EGO membranes. The XRD patterns of EGO membrane (**Figure S8**) can be fitted with two component peaks: GO-1 and GO-2, centred on about 9.1° and 7.6°, respectively, corresponding to interlayer distances of 0.92 nm and 1.16 nm. Since the size of one water molecule is around 0.25 nm, the two fitting peaks represent EGO structure with one (0.92 nm – 0.74 nm = 0.18 nm) and two water monolayers between GO sheets (1.16 nm – 0.74 nm = 0.42 nm). The slightly smaller size of intercalated water molecules is due to their denser state in a confined environment, compared with their existence in the bulk water environment.[5] For EGO membrane immersed for 1 minutes (**Figure S8a**), the GO-1 peak displayed a higher intensity than the GO-2 peak, indicating that majority part of structure was filled with one layer of water molecules. With increasing immersion time (**Figure S8b, c, d, e**), the intensity of GO-1 peak decreased while the intensity of GO-2 peak increased, showing that there is a driving force to produce a two-layered water molecules intercalated EGO gallery. As a comparison, the XRD patterns of CGO membrane with fitted peaks are shown in **Figure S9**. The XRD peak of CGO membrane contains three fitted peaks: GO-1, GO-2, GO-3, where GO-3 is centred on around 6.6° (interlayer spacing = 1.34 nm) which represents three layers of water molecules between CGO sheets. After immersion for 1 day, the XRD pattern changed to a combination of GO-2 and GO-3 peaks, indicating a mixed morphology of two-layer and three-layer water structures. Due to the detection limits in the XRD technique, no peak with larger interlayer distance could be detected but from previous studies, multiple layers of water molecules (up to 6 - 7 nm) could be intercalated between the GO sheets.[5] No GO-3 peak was observed in the XRD pattern of EGO membrane, even after immersion for 1 week (**Figure 2d**), indicating a stable two-layer water molecule structure within EGO membrane.

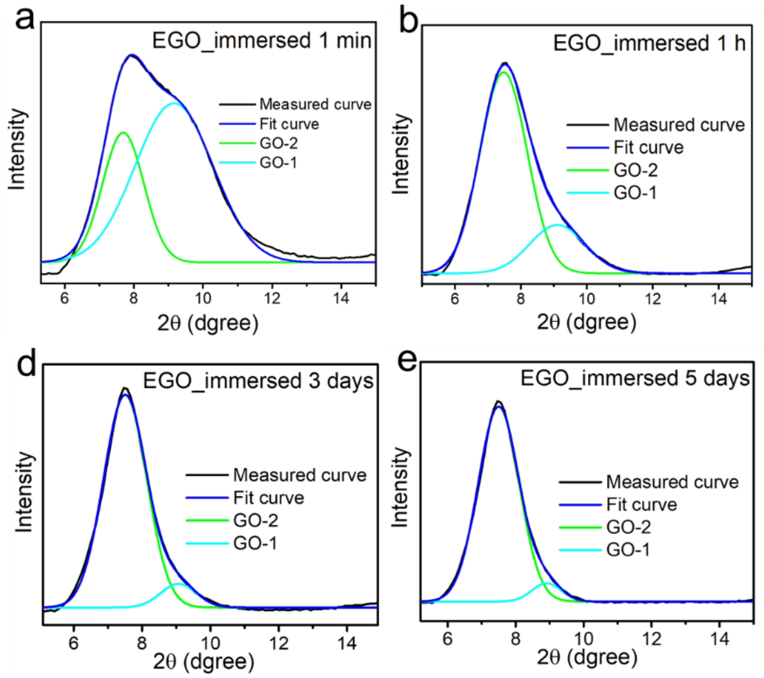

Figure S8. XRD patterns of EGO membrane after being immersed in neutral water for (a) 1 min, (b) 1h, (c) 1 day, (d) 3 days, (e) 5 days, with fitting peaks: GO-1, GO-2, centred at about 9.1° and 7.6°.

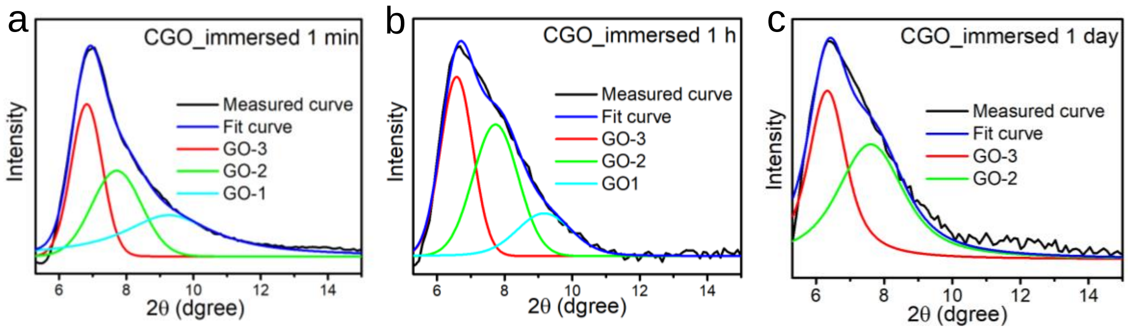

Figure S9. XRD patterns of CGO membrane after being immersed in neutral water for (a) 1 min, (b) 1 h, (c) 1 day, with fitting peaks: GO-1, GO-2, GO-3, centred at about 9.1°, 7.6° and 6.6°, respectively.

ESI-4. Nanofiltration performances of EGO and CGO membranes

Nanofiltration performances of EGO and CGO membranes were tested by pressure-driven filtration setup. The rejection and permeance for NaCl, MgCl, MB and RB solutions were shown in **Figure S10a**. EGO membranes not only had higher rejection for the ions and molecules but also show higher permeance than CGO membranes. In addition, EGO also had a higher rejection for RB molecules in base solution than CGO membrane, shown in **Figure S10b**, which illustrates the better stability of EGO in a base solution compared with a CGO membrane. As a stable graphene oxide membrane in aqueous solution, the EGO membrane shows higher ion and molecular rejection, while simultaneously demonstrating a larger water flux than conventionally used CGO membranes. This combination makes it a promising candidate to be used in water filtration.

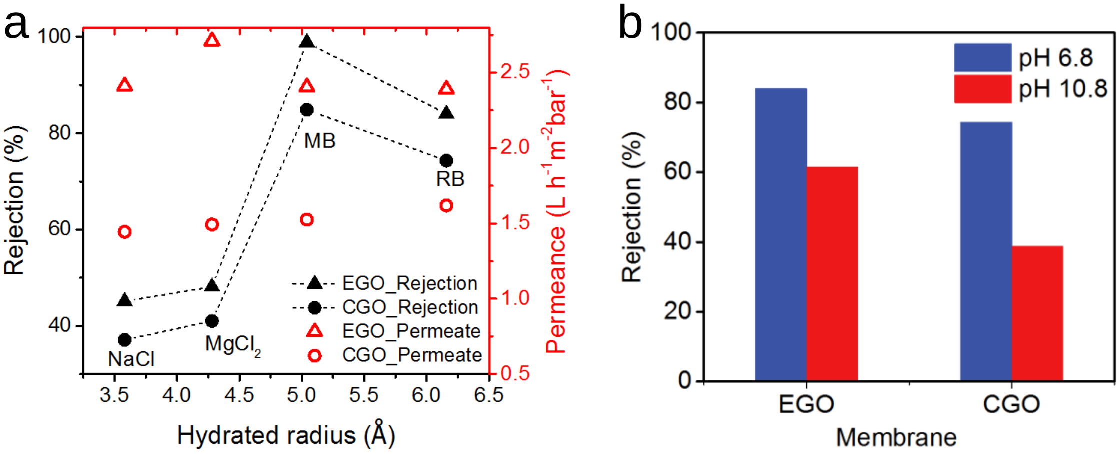

Figure S10. Nanofiltration test of EGO and CGO membrane. (a) Rejection and permeance of EGO and CGO membrane for ions and molecules of different hydrated radius in nanofiltration test. (b) Rejection of EGO and CGO membranes for RB molecules at pH= 6.8 and 10.8.

The EGO membrane was also compared with the result reported by Joshi et al.[6] with the same membrane thickness and concentration of feed solution (**Figure S11**). The EGO membrane shows about three times smaller permeation rate of Na^+ than the reported GO membrane. We would like to note that the ionic sieving performance of GO membranes is greatly affected by testing conditions such as the equipment used and how the GO membrane is prepared. Cautions need to be taken when one attempts to compare the performance under different test conditions, particularly for different GO membranes.

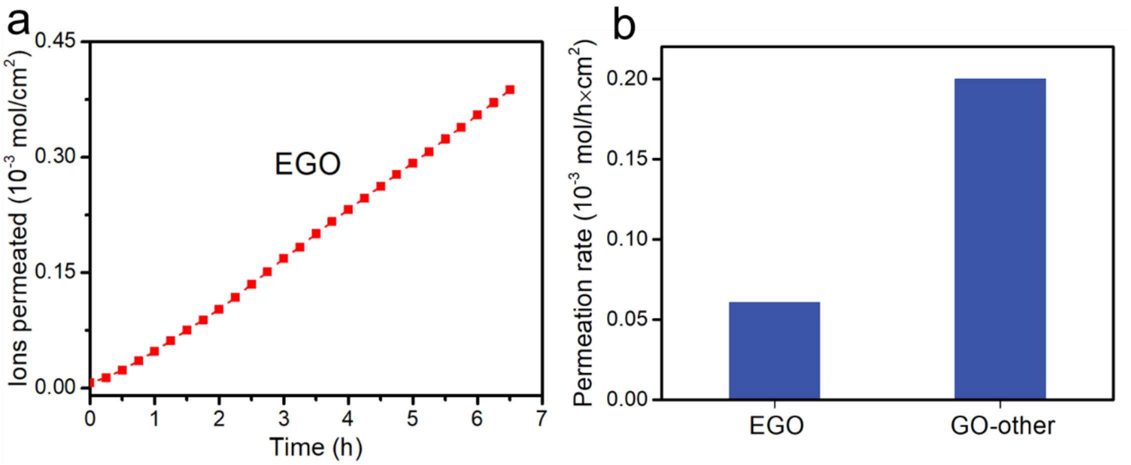

Figure S11. (a) Na^+ ions permeated through EGO membrane with a thickness of 5 µm and concentration of feed solution to be 1M. (b) Comparison of permeation rate for EGO membrane and other GO membrane from the work of Joshi et al.[6]

The rejections to MB molecules were also tested for EGO membranes prepared by different H_2SO_4 concentrations, as shown in **Figure S12**. EGO membranes produced from 12 M H_2SO_4 shows the highest rejection to MB molecules, while higher or lower H_2SO_4 concentrations led to decreased rejections. The concentrations of H_2SO_4 can affect the oxidation level and ultimately the dispersibility of EGO in water. Thus, a number of factors such as exfoliation and oxidation level of EGO, and the void defects caused by the presence of unoxidized graphite could affect the rejection performance of produced EGO membranes. In our case, the EGO prepared from 12 M H_2SO_4 contains the least amount of unreacted graphite as shown in **Figure S1c**, which may lead to less defective membranes.

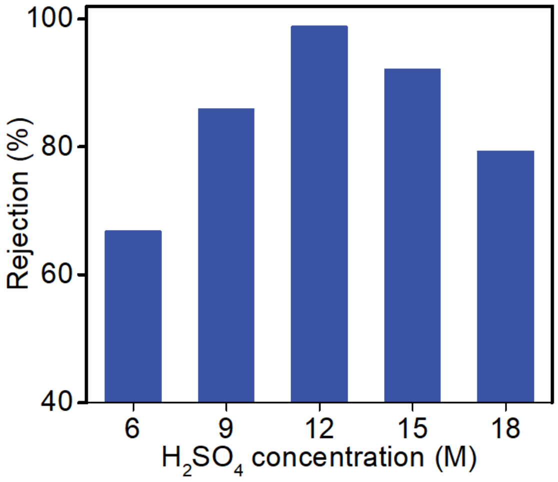

Figure S12. Rejections to MB molecules by EGO membranes produced from different H_2SO_4 concentrations of 6, 9, 12, 15, 18 M.

ESI-5. Structural and chemical characterization

To understand properties of the EGO membranes, the structure and chemistry of EGO were characterized via Raman Spectroscopy, XPS and TGA. **Figure 4a, b** shows Raman spectra of EGO and CGO in the first-order region from 1000 cm^{-1} to 1900 cm^{-1}. The spectra were fitted with Lorentzian functions to show D peak, G peak and D'' peak in the valley between D and G peaks. The prominent peak at around 1590 cm^{-1} is the G peak, which is directly related to the motion of sp^2 atoms in graphene. Another peak in the region of around 1350 cm^{-1} is D peak, which is dependent on the breathing modes of six-atom carbon rings near the defect regions. Therefore, the D peak is often used to indicate the defects in graphene-based materials. The full width at half maximum (FWHM) of D peak and G peak is also an important parameter that reveals the structure of carbon material. The broadening of D and G peaks in graphene oxide are related to the disorder in the graphene plane, resulting from decreasing size of sp^2 aromatic clusters.[7, 8] By comparison of FWHM from **Table 1**, it can be seen that EGO shows a much smaller FWHM of D peak and G peak than CGO. The smaller FWHM of EGO indicates its much larger size of sp^2 domains.

To quantitatively determine the aromatic domain size L_a for CGO and EGO, the intensity ratios of D and G peak I_D/I_G were determined, with the results presented in **Table 1**. CGO and EGO show almost the same value of I_D/I_G intensity ratio. As proposed by Ferrari and Robertson[9], the Raman spectra of disordered carbon material can be explained by a L_a-dependent three-stage model. In Stage One (L_a > 20 Å), I_D/I_G will increase when the aromatic domain size L_a decreases, which is similar to Tuinstra-Koenig (T-K) relationship. When L_a further decreases and becomes Stage Two (L_a < 20 Å), the T-K relation will not be valid since there are decreased signals from sixfold aromatic rings near defects, and as a result, the I_D/I_G ratio will decrease. By considering the dramatic difference of FWHM and an almost similar I_D/I_G ratio of CGO and EGO, it can be speculated that they are classified as different stages. EGO, with larger aromatic domain size, appears to be governed by

Stage One; while CGO is in Stage Two due to its smaller aromatic domain size. The value of L_a can be calculated using a modified Lucchese equation as given below.[8]

$$\frac{I_D}{I_G} = C_A \frac{(r_A^2 - r_S^2)}{(r_A^2 - 2r_S^2)} [e^{-\pi r_S^2/L_D^2} - e^{-\pi(r_A^2 - r_S^2)/L_D^2}]$$

where C_A = 5.43 for 532 nm laser, r_A = 3.1 nm, r_S = 1.0 nm. The calculated L_a for CGO and EGO are 1.3 nm and 11.4 nm, respectively. The larger L_a value of EGO indicates larger aromatic domain size and better long-range order.

Another comparison that can be obtained from the Raman spectra of CGO and EGO is the D'' peak, the appearance of which is correlated to chemical doping or sp^3 bonding. $I_{D''}/I_G$ peak ratio for EGO is more than two times lower than that of CGO. This indicates much less sp^3 bonding in EGO, which is in agreement with the larger calculated aromatic domain size.

Table S2. Percentage of XPS C1s components for CGO and EGO.

	CGO	**EGO**
sp^2	44.7%	48.0%
C=O/C-OH/C-O-C	46.9%	48.5%
COOH	8.4%	3.5%

Figure 4c shows XPS C1s spectra of EGO to analyse its chemical structure. In addition, XPS spectra of CGO is shown in **Figure 4d** for comparison. The spectra were fitted with three peak components: sp^2 (284.4 eV), C=O/C-OH/C-O-C (286.4 eV) and COOH (288.0 eV). Percentages of each components for CGO and EGO were shown in **Table S2**. EGO showed larger percentage of sp^2 bonds (48.0 %) than CGO (44.7 %), which indicates a reduced oxidation degree of EGO. By comparing the percentage of oxygen groups, it can be seen that EGO contains a higher number of C=O/C-OH/C-O-C groups while much lesser percentage of COOH groups than CGO. EGO only shows 3.5 % of COOH groups compared to 8.4 % for CGO. As shown in the thermogravimetric analysis (TGA) curves in **Figure S13**,

EGO exhibits about 30% of weight loss at around 200 °C due to removal of most oxygen groups, which is slightly less than for than CGO. EGO also shows less weight loss in the middle region, between two significant weight losses (around 200 – 500 °C) than CGO (around 200 – 400 °C), likely due to less amount of thermally unstable C=O/COOH groups in EGO. The much higher carbon decomposition temperature for EGO indicates its higher thermal stability after reduction. From the above results, most of the oxygen bonded to graphene plane during oxidation of EGO form epoxy, hydroxyl, or carbonyl groups, with only a small amount further oxidized to carboxylic groups.

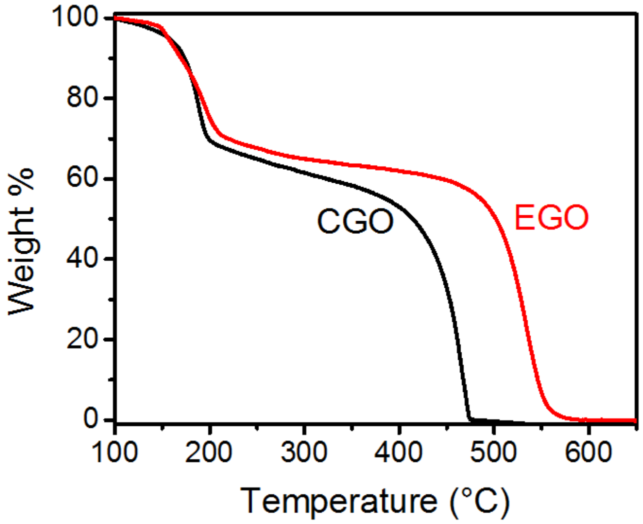

Figure S13. Thermogravimetric analysis (TGA) curves of EGO and CGO in air atmosphere

The elements of EGO and CGO were also analyzed by XPS survey spectra and EDS spectra. **Figure S14** shows XPS survey spectra of EGO and CGO with the element % listed in the inset table. It can be found that EGO and CGO are mainly composed of C and O elements with a minority of S and N elements. EGO exhibits 73.9 at.% C and 25.2 at.% O elements, which is slightly less oxidized than CGO with 71.3 at.% C and 28.1 at.% O elements. The element percentages of EGO and CGO were further analyzed by EDS technique, as shown in **Figure S15** and **Figure S16**, respectively. It is again found that EGO and CGO are mainly composed of C and O elements, which are uniformly distributed across the membranes. The weight percentage of C and O for EGO is 64.3 wt% and 34.3 wt%, respectively which are in agreement with the XPS results.

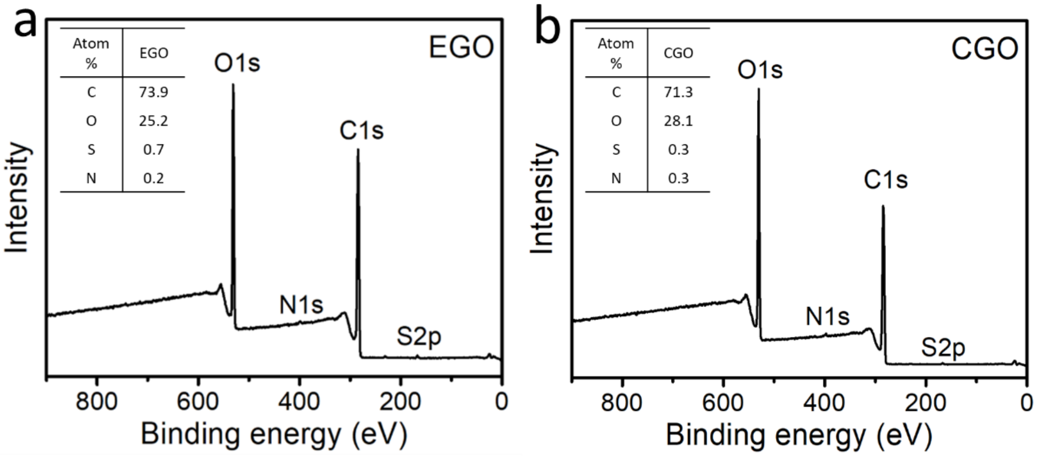

Figure S14. XPS survey spectra of (a) EGO and (b) CGO, with C, O, S, N elements % listed in the inset table.

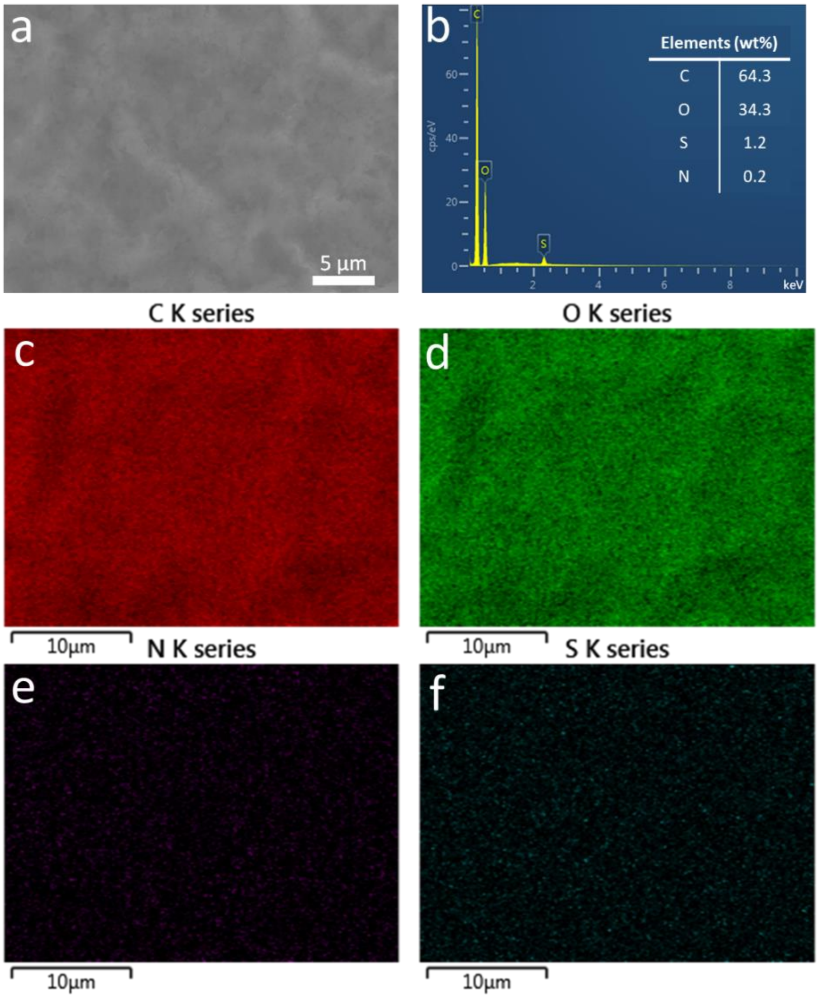

Figure S15. (a) SEM image of EGO membrane surface. (b) EDS spectrum of EGO membrane. EDS element distribution maps of (c) C element, (d) O element, (e) N element, (f) S element.

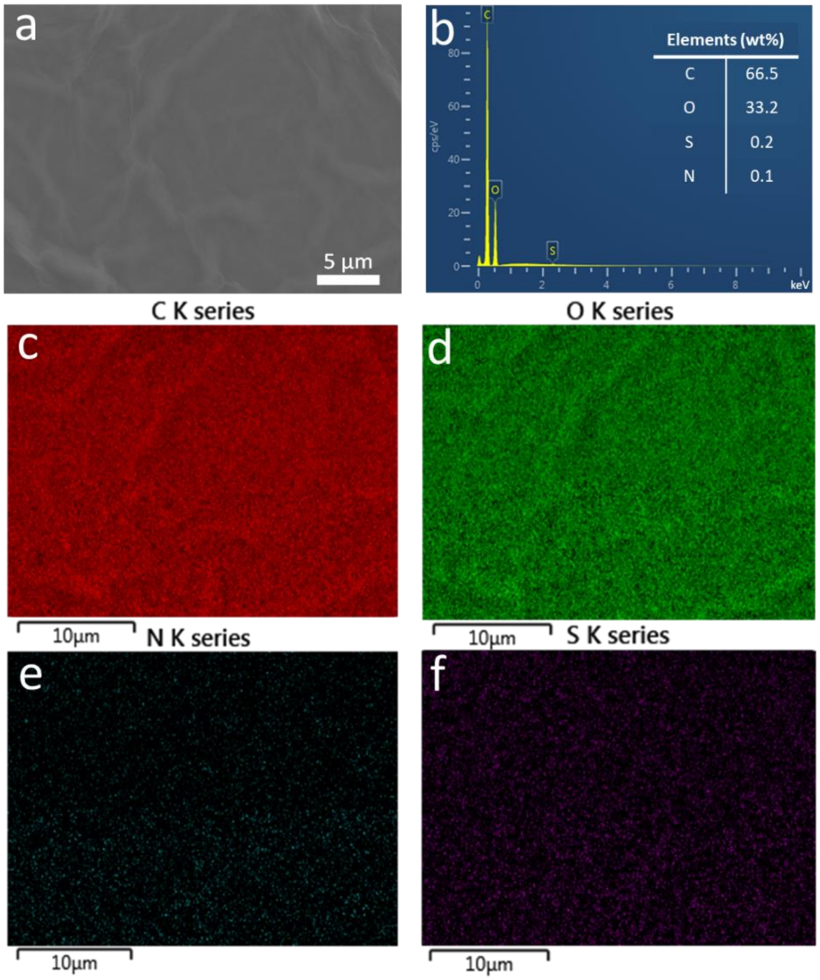

Figure S16. (a) SEM image of CGO membrane surface. (b) EDS spectrum of CGO membrane. EDS element distribution maps of (c) C element, (d) O element, (e) N element, (f) S element.

References:

1. Z. Tian, P. Yu, S. E. Lowe, A. G. Pandolfo, T. R. Gengenbach, K. M. Nairn, J. Song, X. Wang, Y. L. Zhong and D. Li, *Carbon*, 2017, **112**, 185-191.
2. N. I. Kovtyukhova, P. J. Ollivier, B. R. Martin, T. E. Mallouk, S. A. Chizhik, E. V. Buzaneva and A. D. Gorchinskiy, *Chemistry of Materials*, 1999, **11**, 771-778.
3. D. Li, M. B. Muller, S. Gilje, R. B. Kaner and G. G. Wallace, *Nat Nano*, 2008, **3**, 101-105.
4. A. V. Talyzin, T. Hausmaninger, S. You and T. Szabo, *Nanoscale*, 2014, **6**, 272-281.
5. S. Zheng, Q. Tu, J. J. Urban, S. Li and B. Mi, *ACS Nano*, 2017, **11**, 6440-6450.
6. R. K. Joshi, P. Carbone, F. C. Wang, V. G. Kravets, Y. Su, I. V. Grigorieva, H. A. Wu, A. K. Geim and R. R. Nair, *Science*, 2014, **343**, 752-754.
7. A. C. Ferrari, S. E. Rodil and J. Robertson, *Physical Review B*, 2003, **67**, 155306.
8. L. G. Cançado, A. Jorio, E. H. M. Ferreira, F. Stavale, C. A. Achete, R. B. Capaz, M. V. O. Moutinho, A. Lombardo, T. S. Kulmala and A. C. Ferrari, *Nano Letters*, 2011, **11**, 3190-3196.
9. A. C. Ferrari and J. Robertson, *Physical Review B*, 2000, **61**, 14095-14107.